Micro-chemical synthesis of molecular probes on an electronic microfluidic device

Pei Yuin Keng[a,b], Supin Chen[c], Huijiang Ding[a,b], Saman Sadeghi[a,b], Gaurav J. Shah[d], Alex Dooraghi[e], Michael E. Phelps[a,b], Nagichettiar Satyamurthy[a,b], Arion F. Chatziioannou[a,b,e], Chang-Jin "CJ" Kim[f], and R. Michael van Dam[a,b,e,1]

[a]Crump Institute for Molecular Imaging; [b]Department of Molecular and Medical Pharmacology, David Geffen School of Medicine; [c]Biomedical Engineering Department; [e]Biomedical Physics Interdepartmental Program; [f]Mechanical and Aerospace Engineering Department, University of California (UCLA), Los Angeles, CA 90095; and [d]Sofie Biosciences, Inc., Culver City, CA 90230

We have developed an all-electronic digital microfluidic device for microscale chemical synthesis in organic solvents, operated by electrowetting-on-dielectric (EWOD). As an example of the principles, we demonstrate the multistep synthesis of [18F]FDG, the most common radiotracer for positron emission tomography (PET), with high and reliable radio-fluorination efficiency of [18F]FTAG (88 ± 7%, $n = 11$) and quantitative hydrolysis to [18F]FDG (>95%, $n = 11$). We furthermore show that batches of purified [18F]FDG can successfully be used for PET imaging in mice and that they pass typical quality control requirements for human use (including radiochemical purity, residual solvents, Kryptofix, chemical purity, and pH). We report statistical repeatability of the radiosynthesis rather than best-case results, demonstrating the robustness of the EWOD microfluidic platform. Exhibiting high compatibility with organic solvents and the ability to carry out sophisticated actuation and sensing of reaction droplets, EWOD is a unique platform for performing diverse microscale chemical syntheses in small volumes, including multistep processes with intermediate solvent-exchange steps.

molecular imaging | PET probes | synthetic chemistry | lab on a chip | on-chip chemistry

The use of micro-reaction technology in chemistry has grown tremendously over the past several years (1), due primarily to the highly precise control of reaction conditions that is possible through rapid mixing and heat transport, leading to improved reaction speeds and selectivity compared to macroscale approaches (2). Additional advantages include straightforward scale-up of production without changing conditions, and increased safety in dangerous syntheses due to the minute amounts of reagents within the reactor at any given time. A further advantage of microfluidics is the ability to perform reactions in extremely small volumes, which is valuable for many applications, especially when working with scarce reagents, such as isolated proteins or natural products, products of long synthetic pathways, or short-lived radiolabeled radioisotopes where the needed mass quantities are extremely low (3).

Myriad microfluidic platforms have been explored for chemical reactions that can be classified into three basic formats: (*i*) flow-through (or continuous flow), (*ii*) droplet or slug, or (*iii*) batch. In *flow-through* systems, streams of two or more reagents are mixed and reacted by flowing through a residence time unit held at a constant temperature or immersed in a fixed microwave field. Continuous liquid-liquid extraction and other processes have been developed to enable multistep reactions where different solvents are required in different steps (4). *Droplet* and *slug* systems are a variant of flow-through systems, in which individual droplets or slugs (with volumes down to tens of nanoliters) are separated by an immiscible carrier fluid, each acting as an isolated batch microreactor and enabling vastly reduced reaction volumes. Screening assays and optimization studies have been performed in this format (5), but multistep reactions remain challenging. This latter limitation has been addressed with *batch microfluidic* chip designs that use microvalves to isolate small batches of reagents within a chamber. Solvents can be evaporated while solutes remain in the chamber (6), permitting multistep organic synthesis in nanoliter volumes.

Because the primary material used for these latter devices, poly(dimehtylsiloxane) (PDMS), is known to be incompatible with many organic solvents and to absorb or interact with many reagents (7), this platform is inherently limited in its chemical flexibility. Here we describe an alternative platform for batch synthesis at the microscale: electrowetting-on-dielectric (EWOD). Constructed from inorganic materials coated with a perfluoro-polymer layer, these microfluidic chips provide much greater compatibility with diverse reagents and reaction conditions for microscale chemical synthesis. EWOD devices belong to a class of two-dimensional (2D) systems that manipulate droplets using their surface tension (8). A typical device consists of two parallel plates: (*i*) a substrate patterned with electrodes and coated with dielectric and nonwetting layers, and (*ii*) a cover plate coated with a conductor (to act as a ground electrode), dielectric and nonwetting layers. Droplets are sandwiched into a disc shape between the plates, and electrical potential is applied to individual or multiple electrodes to achieve unit operations such as droplet generation, transport, splitting, and merging (9). Liquid manipulation is performed electronically, eliminating the need for moving parts such as pumps and valves, and simplifying the chip and the external control system. It is possible to integrate additional electronically controlled functions into the chip such as sensors to monitor liquid volumes (10) and composition (11) as well as heaters and temperature sensors for heating liquid droplets or evaporating solvent (12). The open structure of EWOD chips (without the use of surrounding oil medium) is particularly advantageous in achieving rapid solvent evaporations and solvent exchange. Such processes greatly extend the sophistication of chemical syntheses that can be performed on-chip by enabling multistep reactions. Though generally used for manipulation of aqueous samples and biochemical assays (8) EWOD chips can manipulate organic solvents (13) and ionic liquids (14) for performing chemical reactions.

We demonstrate here multistep chemical synthesis in EWOD chips involving volatile organic solvents such as acetonitrile (MeCN) to produce 2-[18F]fluoro-2-deoxy-D-glucose ([18F]FDG),

the most commonly used radiotracer for imaging of living subjects with positron emission tomography (PET) (15, 16). It has previously been shown, with flow-through systems working with relatively large volumes (e.g., 0.5–1.0 mL), that changing from macroscale to microscale geometry leads to dramatic acceleration of reactions in the synthesis of [18F]FDG (17, 18) and other PET tracers labeled with short-lived radioisotopes (19). Performing the chemistry in small volume batches in the 40 nL–60 μL range (6, 20, 21) offers further additional advantages, including: (*i*) reduced precursor consumption, (*ii*) accelerated heating and cooling due to reduced mass of liquid, and (*iii*) increased integration of overall synthesis processes (including [18F]fluoride activation) onto the compact chip. It is possible to work at this scale due to the extremely minute mass of tracers needed for PET imaging (e.g., 6 pmol for typical human scan). Other potential advantages (not yet established experimentally) include enhanced reaction kinetics (by increased concentration of [18F]fluoride), reduced radiolysis (due to confinement of reaction mixture in geometries with dimensions less than the positron range), simpler purification, and increased specific activity (ratio of the radiolabeled to the nonradiolabeled form). The EWOD digital microfluidics described here provides a unique platform for synthesis at these small scales (100 nL–20 μL)—one that overcomes the serious limitations observed in PDMS radiosynthesis chips such as poor chemical compatibility, low synthesis repeatability, high loss of radioactivity (up to 95% of [18F]fluoride), and long evaporation times through PDMS membranes (20). EWOD devices have the additional advantage of digitally programmable fluid pathways that combined with their high chemical and temperature compatibility (22), could readily be configured for a wide variety of microscale batch organic syntheses, optimization, or screening studies.

Results and Discussion

EWOD Chemistry Chip. The structure, electrode design, and fabrication of the EWOD chemistry chip are shown in Fig. 1, Fig. S1. Droplets of reagents are sandwiched between two glass plates separated by a gap of 150 μm. The base plate is patterned with an array of electrode pads to control the movement and operations with droplets within the chip. The majority of these electrodes control transport of reagent droplets by sequential activation along "virtual channels" from two reagent loading sites at the edge of the chip to the central circular reaction site. The elec-
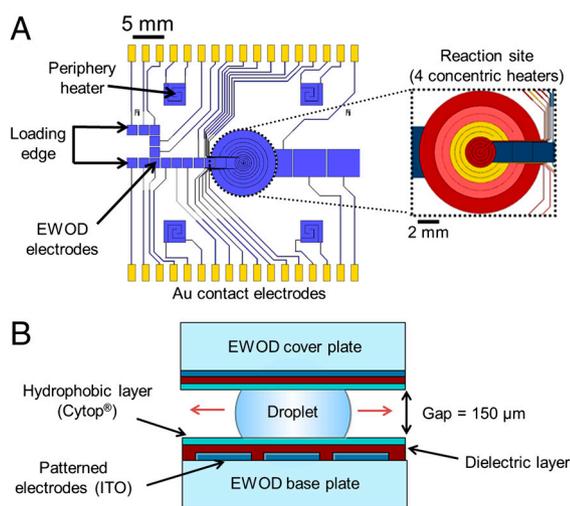
trode pads within the reaction site are designed to be multifunctional, capable of resistive Joule heating and thermistic temperature sensing in addition to droplet transport (12). The cover plate is coated with a blanket electrode, which electrically grounds the droplets. Both of the plates are coated with a dielectric layer (silicon nitride used) to electrically insulate the droplets from the electrodes, and a layer of Cytop® to enhance the EWOD effect. The transparent conductor indium tin oxide (ITO) is used for electrodes and connection lines to facilitate visualization of the process occurring within the chip. However, the connection lines leading to heating electrodes are made of gold, which has higher conductivity than ITO, to ensure that most of the voltage drop (and heating effect) occurs on the heater rather than on the connection lines.

The central 12 mm-diameter reaction site is composed of multifunctional electrodes and can be used to control the temperature of liquid volumes up to about 17 μL. The reaction site comprises four concentric heating rings, independently capable of feedback temperature control, for reaction and evaporation steps. The concentric design enables centering of the reaction droplet by EWOD, and provides more accurate temperature measurement and uniform temperature control, especially as the droplet shrinks during evaporation steps. More specifically, power to the outer heating rings is lowered or cut off successively as each ring senses its surface being dried. If not divided into multiple heating rings, a single circular heater would sense one average temperature over its entire area. As the liquid droplets shrink, the heater surface outside the liquid would be overheated while the liquid would be underheated.

These chip features support a small set of "unit operations," sequences of which are combined to perform multistep chemical syntheses. The operations include: (*i*) reagent transport, (*ii*) mixing/redissolving, (*iii*) reaction at elevated temperature, and (*iv*) evaporation. (See Fig. S2).

Radiosynthesis of [18F]FDG on EWOD Chip. The synthesis of [18F]FDG was performed according to the method developed by Hamacher, et al. (23), adapted for μL-scale reactions on the EWOD chip (Fig. 2). Briefly, the original synthesis involves activation of the [18F]fluoride ion, followed by fluorination of the mannose triflate precursor at elevated temperature in MeCN, and finally deprotection at elevated temperature with hydrochloric acid (HCl).

[18F]fluoride is produced from the $^{18}O(p,n)^{18}F$ nuclear reaction by bombardment of an [18O]H2O target by a proton beam in a cyclotron. Herein, we worked with radioisotope concentrations of about 0.2 mCi/μL, though higher concentrations (1 mCi/μL or more) can readily be obtained. For example, using a miniature anion exchange cartridge, rapid and efficient trapping of >800 mCi from a cyclotron target volume has been achieved, followed by elution of nearly all activity into only 5 μL of K_2CO_3 (20). We intend to operate at high levels of radioactivity when the chip is further automated. The [18F]fluoride must be activated prior to fluorination of the precursor by disrupting the strong water-fluoride interaction, which is most commonly achieved by a solvent-exchange process using an anion exchange cartridge and/or evaporation in the presence of a phase-transfer catalyst. Activation in Hamacher's synthesis (and many others) is achieved by forming the [18F]KF/$K_{2.2.2}$ complex and adding acetonitrile, which forms a low-boiling-point azeotrope with water and thereby facilitates the removal of water via evaporation. Translation of the associated evaporation steps to EWOD is straightforward as the open sides of the EWOD chip facilitate the removal of solvent vapor from the droplet. However, the heated reactions in volatile solvents (e.g., the fluorination in MeCN, bp = 82 °C) are more challenging to perform in EWOD as the open sides lead to significant unwanted evaporation and unreliable synthesis. At the macroscale, the reaction vessel is typically closed, causing vapor pressure to build up within the vessel

Fig. 1. (*A*) EWOD microchip with four concentric heaters (dashed circle) with a maximum volume of 17 μL. Inset shows magnified area of the heater with four concentric individually controlled resistive heating rings. (*B*) Schematic side view of the EWOD chip sandwiching a reaction droplet between two plates coated with ITO electrodes, a dielectric layer, and a hydrophobic layer of Cytop (not to scale).
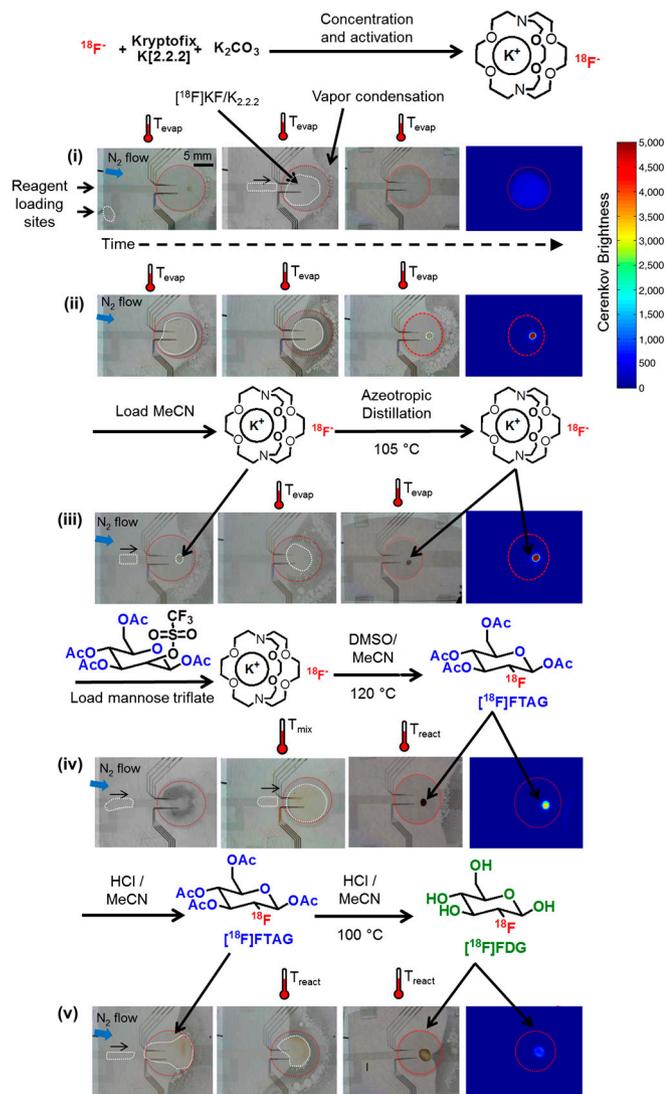
Fig. 2. Sequence of photograph images with and the corresponding Cerenkov images (blue background) and the synthetic scheme of the multistep radiosynthesis performed on EWOD. For clarification, the heater region is outlined with a red circle, the droplet is outlined with white dashes, the blue arrow illustrates the needle position and direction of nitrogen flow, and the activation of the heater is indicated by the thermometer symbol with adjacent temperature. (*i*) Edge loading of the $[^{18}F]KF/K_{2.2.2}$ complex onto the chip and transport to the heater via EWOD; (*ii*) Concentration of the $[^{18}F]KF/K_{2.2.2}$ complex via evaporation; (*iii*) Exchange of solvent to anhydrous MeCN followed by several cycles of azeotropic distillation; (*iv*) Loading of mannose triflate (precursor) and mixing with the dried $[^{18}F]KF/K_{2.2.2}$ by heating at moderate temperature; followed by fluorination of mannose triflate; (*v*) Addition of droplets containing a mixture of HCl/MeCN to the crude $[^{18}F]FTAG$ intermediate to perform hydrolysis to form $[^{18}F]FDG$. The color legend on the right indicates the brightness of the Cerenkov light. Qualitatively, Cerenkov images confirmed that the radioactivity is always confined to the droplet in steps where liquid is present in every step of the synthesis.

and limit the amount of solvent that can evaporate. Sealing the edges of the EWOD chip was unsuccessful, simply resulting in redistribution of the entire liquid volume from the reaction droplet to cooler parts of the chip.

A common technique employed to reduce evaporation in EWOD devices is to fill the device with an immiscible, high-boiling-point liquid such as fluorinated oil which surrounds the droplets (24). However, for many chemical syntheses, this approach is not practical due to the miscibility of oil with many organic solvents, and the difficulty in efficiently separating the oil from the reaction product. Furthermore, for multistep syntheses where

solvent-exchange is needed, the oil completely prevents the possibility of evaporative removal of solvent. Reduction of evaporation can also be achieved by surrounding droplets with a pressurized gas medium, which reduces the diffusion constant of vapor through the medium (25).

Another strategy that has been reported is to perform the reaction in exotic, nonvolatile solvents such as ionic liquids as has been reported for the synthesis of tetrahydroquinolines on EWOD chips (26). Ionic liquids have been used in the (macroscale) synthesis of $[^{18}F]FDG$, and in fact eliminate the need for an initial drying step to activate the $[^{18}F]$fluoride (27). We elected not to use ionic liquids because this approach often requires tailoring the ionic liquid for a specific chemical reaction and also could make isolation of final product challenging. (28) To facilitate rapid translation of PET tracer syntheses into the microfluidic chip and leveraging the existing knowledge base of protocols based on traditional organic solvents, we explored using a mixture of 1:4 DMSO:MeCN (vol/vol) instead of pure MeCN. DMSO (bp = 182 °C) evaporates more slowly and maintains complete solvation of the reaction mixture throughout the synthesis. DMSO has numerous advantages over MeCN including high polarizability, fast reaction rates, and the ability to perform chemical reactions at higher temperatures (29), but is not preferably used in conventional macroscopic synthesis due to the difficulty in removing it after the synthesis. At the microscale, we found only residual amount of DMSO at the end of the reaction due to the extremely small starting volume. The residual DMSO did not adversely affect the subsequent hydrolysis step nor did it generate toxic byproducts under the harsh (high temperature and acidity) reaction conditions (see *SI Text*). Moreover, the residual amount was below the acceptable limits for human use and seemed not to adversely affect the image quality or health of the mouse during micro-PET imaging.

This minor but critical modification in the chemistry enabled systematic screening of reaction conditions as each parameter could be controlled independently unlike the case of evaporating droplets of volatile solvents where the concentration, temperature, and reaction time are more tightly coupled. Specific screening studies are discussed in detail in the *SI Text* and in Fig. S3 and S4.

Optimized Synthesis. The following sections summarize all steps of the radiosynthesis of $[^{18}F]FDG$ implemented in the EWOD chip, including results at each step obtained by standard analytical techniques as well as Cerenkov imaging—a technique to obtain qualitative distribution of radioactivity on EWOD chip in situ. Compared to the previously reported Cerenkov imaging system (30), the setup here used a rotatable mirror to switch between Cerenkov and bright-field imaging subsystems, enabling optimization of each imaging modality and permitting the Cerenkov CCD camera to be shielded from direct gamma irradiation to reduce noise in the images (Fig. S5). Details of the Cerenkov imaging setup, radioactivity calibration, and step-by-step quantitative analysis of EWOD radiotracer synthesis will be published elsewhere.

$[^{18}F]$fluoride activation. The solution of no-carrier-added $[^{18}F]$ fluoride in $[^{18}O]H_2O$ was premixed with a solution of complexing agent [Kryptofix $K_{2.2.2}$ and K_2CO_3 in MeCN:H_2O (95:5, vol/vol)]. The optimal volume ratio of these solutions was investigated to maximize the concentration of radioactivity per droplet without compromising the fluorination efficiency due to the increased water content. We found that up to 50% $[^{18}F]$fluoride/$[^{18}O]H_2O$ could be used, enabling loading up to ~1.7 mCi at a time into the chip. (About 0.05–0.2 mCi of the final tracer is needed for preclinical imaging in a mouse.) Droplets of the $[^{18}F]KF/K_{2.2.2}$ mixture in H_2O/MeCN (1:1, vol/vol) were sequentially loaded onto the EWOD chip using a micropipette,

transported to the heater and evaporated at 105 °C (Fig. 2, *i*). During evaporation, a stream of nitrogen was introduced into the chip via a needle aligned parallel to the gap within the EWOD chip. The nitrogen flows around the droplet to facilitate the removal of solvent vapor out of the chip and thereby increases the efficiency of the drying process. This flow likely helps to maintain a high evaporation rate by avoiding the buildup of partial pressure of vapor near the droplet-air surface as evidenced by the absence of condensation around one half of the droplet when the nitrogen flow is turned on (Fig. S6). Nitrogen flow also seems to help prevent catastrophic bursting of droplets heated near or above the solvent boiling point. After the solvent was evaporated from the loaded solution, the process was repeated to double the amount of radioactivity loaded into the chip. Cerenkov imaging confirmed that the radioactivity remained localized within the reaction heater throughout the loading and evaporation steps (Fig. 2, *ii*).

Azeotropic distillation. After loading and drying of the aqueous [18F]fluoride mixture, further removal of residual water was achieved via three cycles of azeotropic distillation. For each, additional MeCN droplets were transported to the reaction site via EWOD and evaporated at 105 °C under a nitrogen flow. After the final azeotropic distillation step, the spatial distribution of the dried [18F]fluoride complex on-chip was determined via Cerenkov imaging (Fig. 2, *iii*), in order to optimize the volume of solvent needed to cover and thus resolubilize all of the dried [18F]KF/K$_{2.2.2}$ residue in the subsequent radio-fluorination step.

Nucleophilic substitution (radiofluorination). Based on the Cerenkov image, droplets of precursor solution were loaded onto the chip and transported to the heater electrode until the combined droplet covered all of the radioactive area. Very little mixing of the radioactive solute into the precursor solution was observed (via Cerenkov imaging) if the droplet remained at room temperature for relatively long times (e.g., 5–10 min). By heating to 60 °C for 3 min, a uniform distribution of radioactivity throughout the droplet was observed (Fig. 2, *iv*), indicating effective dissolution and mixing of the [18F]KF/K$_{2.2.2}$ into the precursor droplet. We suspect this mixing action occurs primarily through convection, perhaps arising due to cooling from the cover plate and evaporation at the droplet edge, as suggested by Marchand, et al. (14). After mixing, the fluorination reaction was performed at 120 °C for 10 min to obtain the intermediate product 2-deoxy-2-[18F]fluoro-1,3,4,6-tetra-*O*-acetyl-beta-D-glucopyranose ([18F]FTAG). During the fluorination reaction, the droplet shrank from about 16 µL to 1 µL, presumably due to loss of most of the MeCN and some of the DMSO. Radio-thin-layer chromatography (TLC) analysis showed the conversion of [18F]fluoride to [18F]FTAG to be high and repeatable (88 ± 7%, n = 11) (Fig. 3).

Hydrolysis. The intermediate [18F]FTAG was hydrolyzed under acidic conditions to produce the final product, [18F]FDG. A mixture of 1N HCl solution and MeCN was loaded, transported to the reaction site, and heated to 100 °C for 10 min. Analysis via Cerenkov imaging (Fig. 2, *v*) showed that the entire radioactivity remained within the boundaries of the reaction droplet, suggesting effective utilization of the radioactivity in all steps after drying. The conversion efficiency of the overall radiosynthesis was analyzed via radio-TLC developed in MeCN/H$_2$O (95:5 vol/vol). The radio-TLC (Fig. 3*A*) showed the three peaks that are normally observed in the conventional synthesis, namely: (*i*) unreacted [18F]fluoride, (*ii*) [18F]FTAG, and (*iii*) [18F]FDG. This result showed that the hydrolysis of [18F]FTAG was successful under the optimized acidic condition despite the presence of residual DMSO in the hydrolysis reaction. In order to confirm complete hydrolysis of [18F]FTAG to [18F]FDG, a second TLC

of the crude product was developed in hexanes/ethyl acetate (50:50 vol/vol). This method provides distinct separation between the various hydrolysis intermediates and the [18F]FDG product, thus enabling development of a quantitative hydrolysis condition on EWOD chip. Prior to optimization of the hydrolysis reaction conditions, we observed a significant amount of partially-hydrolyzed product via this second TLC method that was not separated in the standard TLC (in MeCN/H$_2$O) (Fig. S7). It is unclear whether other microfluidic studies of [18F]FDG synthesis have explored the degree of completion of hydrolysis in detail.

Quality Control (QC) Analysis of [18F]FDG. Following the synthesis and purification in a custom miniature cartridge (Fig. 3*B*, SI Text), the formulated [18F]FDG product (approximately 250 µL for multiple-mouse imaging) was subjected to the stringent set of standard quality control procedures recommended for testing purity and safety prior to injection into humans (31), including the Kryptofix colorimetric TLC test, pH test, residual solvent analysis via gas chromatography (GC) and radiochemical purity analysis via high performance liquid chromatography (HPLC) and radio-TLC. Due to the higher sensitivity and other advantages of potassium permanganate staining (32), we use this method to test the concentration of Kryptofix rather than the more common iodine staining. Additional tests such as filter-integrity, bacterial endotoxin, and pyrogenicity tests, were not performed, as there is no expected difference in outcome compared with conventional synthesis.

The final product solution was found to be clear and free of particulates. The concentration of residual Kryptofix was determined to be <4 µg/mL, well below the 50 µg/mL allowable limit set by the United States Pharmacopeia (USP). The pH of the final product was measured using a calibrated pH meter to be 7.2. Furthermore, quantitative GC analysis showed that the [18F]FDG product contained 870 ppm of DMSO, 115 ppm of ethanol and undetectable level of acetonitrile. The detection limit is estimated to be <20 ppm, which is sufficient given that the maximum allowable concentration of these solvents are generally in the range of hundreds to thousands ppm. The USP allowable limits for DMSO, ethanol, and acetonitrile are 5,000 ppm, 5,000 ppm, and 400 ppm, respectively. Though we did not expect significant DMSO side products in the synthesis due to the milder conditions and shorter time scales than generally needed for decomposition, we quantitatively analyzed the residual amounts of these toxic side products (33). Several [18F]FDG samples were tested and none of these compounds were detected (Fig. S8*A*). Radiochemical purity was determined by radio-TLC as above and by isocratic
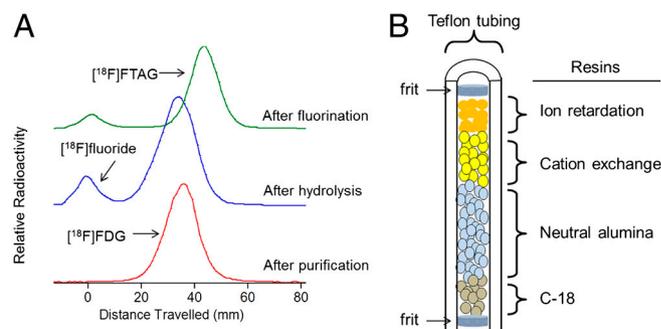

Fig. 3. (*A*) Stack radio-TLC chromatogram of the crude [18F]TAG (green trace), crude [18F]FDG (blue trace), and purified [18F]FDG (red trace) from a typical on-chip synthesis. The radio-TLC profile of the purified [18F]FDG showed >99% chemical purity after passing through the custom made cartridge shown in (*B*), with 88% purification efficiency. (*B*) A schematic diagram of the custom made cartridge comprised of ion retardation, cation exchange, neutral alumina and C-18 resins packed within a 760 µm diameter perfluoroalkoxy tube.

radio-HPLC (see Fig. S8*B*). It should be noted that if the tracer was actually to be used in humans, each dose could be diluted to about 10 mL volume, further reducing all the impurity levels reported here.

Overall radiochemical yield was found to be $22 \pm 8\%$ ($n = 11$). Other work in batch microfluidics has not clearly reported the yield or the repeatability; however, the loss of radioactivity due to interaction with the PDMS material is described as being between 5–95% (20), so our result represents a tremendous improvement in repeatability. Though the yield obtained is somewhat lower than typically obtained in macroscale synthesis, the compact device size, flexibility of digital control, and ability to work at small volumes offer unique advantages. The total time for this proof-of-concept synthesis was ~60 min, with an additional 15 min for off-chip purification. The time is longer than other chip-based and macroscale approaches due to the many manual steps of loading reagents, activating droplet operations, and product droplet collection. We are currently developing technology for automated reagent loading and product extraction and anticipate a reduction to ~30 min, with further reductions expected by optimizing the heating control. Although several groups have reported batch microfluidic synthesis of PET tracers, to the best of our knowledge, none have reported data on the repeatability of the radiosynthesis on-chip, which is a crucial factor in translating this technology to other users, commercialization, and eventual clinical use. Furthermore, these previous studies have not reported detail, quantitative quality control analysis of the tracer produced in the chip.

Micro-PET Imaging. To further validate the quality of the [18F]FDG synthesized on-chip, the in vivo biodistribution was examined by imaging a lymphoma xenograft-bearing mouse with micro-PET/CT. As shown in Fig. 4, the image of the mouse exhibits the expected uptake of [18F]FDG in the tumor, heart, kidneys, and bladder. Quantitative analysis of the overall biodistribution of [18F]FDG synthesized on the EWOD chip was comparable to the biodistribution in the same mouse using [18F]FDG obtained from the UCLA Biomedical Cyclotron facility that provides [18F]FDG for patient care under cGMP (Table 1). The differences in the tumor uptake can be explained by the growth in tumor size between the 2 d of imaging.

Conclusions

The EWOD-based micro-reaction technology reported here was optimized for performing unit operations (transporting, heating, mixing, and solvent exchange) on organic or aqueous droplets, which can be combined to perform multistep synthesis at the microscale. Using this platform, we successfully demonstrated
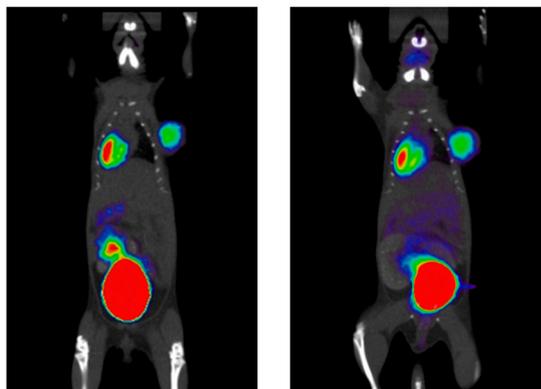

Fig. 4. Small animal PET and CT images of a mouse bearing a lymphoma xenograft (right shoulder) after administration of [18F]FDG prepared on EWOD chip (left), and [18F]FDG prepared at the UCLA Biomedical Cyclotron facility (right). Injections and static scans (10 min duration, 1 h postinjection) were performed on the same mouse on consecutive days.

Table 1. Biodistribution (% uptake) of [18F]FDG in the tumor and other organs relative to the whole body as determined from micro-PET image analysis. The tumor had grown approximately 30% after the first study, in part explaining the higher uptake seen in the second study

Organ	% Uptake (EWOD FDG)	% Uptake (cyclotron facility FDG)
Whole body	100	100
Heart	1.6	1.5
Tumor	2.8	4.6
Left kidney	1.2	1.2
Right kidney	1.2	1.3
Bladder	43.4	43.5

the synthesis of [18F]FDG with high and reliable fluorination efficiency ($88 \pm 7\%$, $n = 11$) and quantitative hydrolysis with $22 \pm 8\%$ ($n = 11$) radiochemical yield of the purified product, [18F]FDG. Doses of [18F]FDG sufficient for multiple animal imaging were prepared on-chip, subjected to quality control testing, and the in vivo biodistribution of chip-produced [18F]FDG was validated.

This work demonstrates that EWOD can serve as a microchemistry platform allowing the use of traditional solvents. The translation of radiosynthesis and other multistep chemical processes into the EWOD format is therefore facilitated because significant changes in the chemical synthesis are not required. This versatile platform could readily be used to synthesize additional PET tracers, and potentially form the basis of a technology platform for on-demand production of diverse tracers leveraging the inexpensive supply of [18F]fluoride from the worldwide network of PET radiopharmacies. With further development of preconcentration technologies (20) to enable on-demand dispensing of desired radioactivity, a shipment of [18F]fluoride could supply multiple synthesis runs. Furthermore, the EWOD platform could be extended to small-scale production or optimization studies of a variety of other types of molecules involving scarce or expensive reagents that could benefit from small-volume synthesis.

Compared to other microfluidic approaches for batch chemical synthesis such as PDMS devices, EWOD provides enhanced versatility due to construction from chemically inert materials with high temperature stability, and the flexibility of a single chip design to implement different multistep reaction protocols via electronically programmed "virtual channels" and a small set of unit operations.

Materials and Methods

EWOD Chip Operation. The EWOD chip was fabricated according to previously reported methods (34) (Fig. S1). The chip was operated inside a dark enclosure behind lead shielding to enable Cerenkov imaging. Electrical connections were fed into the enclosure through a 0.5 m-long black tube to limit light leakage (Fig. S5). For EWOD actuation, a 10 kHz signal was generated (33220A waveform generator, Agilent Technologies) and amplified to 100 V_{rms} (Model 601C, Trek). Individually addressable relays (AQW610EH PhotoMOS relay, Panasonic) applied the voltage selectively to desired electrodes to move the liquid droplet. The relays were controlled by a LabVIEW program using a digital I/O device (NI USB-6509, National Instruments). The chip's multifunctional electrodes were connected via a switch to alternate between EWOD actuation or heating and temperature measurement. To independently maintain precise feedback-controlled temperatures over the reaction site's four individual heaters, a multichannel heater controller and driver were built (see SI Text for details of control algorithm).

Reagents. Anhydrous acetonitrile (MeCN, 99.8%), anhydrous dimethyl sulfoxide (DMSO, 99.9%), potassium carbonate (99.9%), mannose triflate for PET imaging and 4,7,13,16,21,24,-hexaoxa-1,10, diazobicyclo(8.8.8) hexacosane 98% (Kryptofix K2.2.2), hexanes, and ethyl acetate were purchased from Sigma-Aldrich and used as received without further purification. 1N HCl (certified, Fisher Chemicals) was purchased from Fisher Scientific and used as received. No-carrier-added [18F]fluoride ion was obtained from the UCLA Biomedical Cyclotron Facility by irradiation of 97% 18O-enriched water with an

11 MeV proton beam using an RDS-112 cyclotron (Siemens). GC standard reagents with >99.5% purity were purchased from Aldrich, Acros Chemicals and Tokyo Chemical Industry and used as received.

General Radiosynthesis Procedure on EWOD Chip. 50 μL (11 mCi) of the aqueous [^{18}F]fluoride ion was added to a 50 μL mixture of $K_{2.2.2}$ (26 mM) and K_2CO_3 (7 mM) in MeCN:H_2O (95:5 vol/vol) to achieve a radioactivity concentration of ~120 μCi/μL. In a typical multistep radiosynthesis on EWOD chip, four droplets of [^{18}F]KF/$K_{2.2.2}$ complex (2 μL each) were pipetted to the edge of the EWOD chip, then transported to the reaction site by EWOD actuation. The 8 μL [^{18}F]KF/$K_{2.2.2}$ droplet was heated to 105 °C within 1.5 min (i.e., 1.3 °C/sec ramp rate) and held at 105 °C for 1 min to evaporate the solvent. The loading and evaporation processes were repeated to achieve a total of 16 μL [^{18}F]KF/$K_{2.2.2}$, corresponding to about 2 mCi of radioactivity on-chip. The [^{18}F]KF/$K_{2.2.2}$ complex was dried via azeotropic distillation by transporting four MeCN droplets (3 μL each) through the first loading edge into the heater site and heated at 105 °C for 1 min. Azeotropic distillations with 12 μL of MeCN were repeated three additional times. To the dried [^{18}F]KF/$K_{2.2.2}$ residue, two droplets of mannose triflate in DMSO (2 μL each; 104 mM) and four droplets of MeCN (3 μL each) were added by pipetting onto the EWOD chip through the second loading edge site. The reaction droplet was heated at 60 °C for 3 min to induce mixing of the dried [^{18}F]KF/$K_{2.2.2}$ residue throughout the precursor solution. Then, the reaction mixture was gradually heated from room temperature to 120 °C over a period of 10 min to perform the fluorination reaction. To the crude [^{18}F]FTAG droplet, five droplets of 1N HCl/MeCN 50:50 (3 μL each) were added and transported to the heater region and heated at 100 °C for 10 min for the deprotection reaction. After synthesis, the cover plate was removed and the crude [^{18}F]FDG product was extracted using 40 μL of H_2O for radio-TLC analysis and cartridge purification. The crude [^{18}F]FDG was passed through the custom-built miniature cartridge and washed with 250 μL of water to collect the final [^{18}F]FDG product.

Analysis and QC of [^{18}F]FDG. The radio-fluorination and hydrolysis efficiencies of [^{18}F]FDG were determined by TLC on silica gel plates using 95:5(vol/vol) MeCN/H_2O (mobile phase 1) or 50:50 (vol/vol) hexanes:ethyl acetate (mobile phase 2). The radioactivity distribution was scanned with a γ-counter (Mini-GITA star, Raytest). For mobile phase 1, the retention factors (R_f) of [^{18}F]fluoride (peak at baseline), [^{18}F]FDG (peak at 33 mm), and [^{18}F]FTAG (peak at

46 mm) were 0.00, 0.47 and 0.65, respectively (Fig. 3*A*). With mobile phase 2, both the unreacted fluoride and [^{18}F]FDG remained on the baseline ($R_f = 0$), while the partially hydrolyzed intermediate travelled from the baseline (Fig. S7*B*). Methods to implement standard QC testing are described in the SI Text.

Micro-PET Imaging and [^{18}F]FDG Biodistribution. A 250 μL batch of purified [^{18}F]FDG was divided into four separate mouse doses, and formulated with saline solution (0.9% wt/vol of NaCl) to reach a total volume of 100 μL in each dose prior to injection for micro-PET imaging. A SCID mouse was injected subcutaneously with 1–5 million BC-1 lymphoma cells (50 μL mixed with 50 μL Matrigel) ~2 w before imaging. The xenograft-bearing mouse was injected with 38 μCi of [^{18}F]FDG via tail vein injection. Following 1 h delay for uptake and nonspecific clearance, the mouse was imaged for 10 min in a small animal PET scanner (MicroPET Inveon, Siemens), followed by a microCT scan (microCAT II, Siemens). The microPET and microCT scans were coregistered to yield a single image that were displayed using AMIDE (35) and images were reconstructed using a 3D filtered back-projection reconstruction algorithm for quantitation. Regions of interest were drawn to calculate ratio of tumor uptake to soft tissues. For comparison, [^{18}F]FDG synthesized at the UCLA cyclotron facility was injected into the same mouse on the subsequent day for microPET imaging under similar conditions. These animal studies were carried out under protocols approved by the Chancellor's Animal Research Committee at the University of California, Los Angeles.

1. McMullen JP, Jensen KF (2010) Integrated microreactors for reaction automation: new approaches to reaction development. *Annu Rev Anal Chem* 3:19–42.
2. Geyer K, Codée JDC, Seeberger PH (2006) Microreactors as tools for synthetic chemists —the chemists' round-bottomed flask of the 21st century? *Chemistry—A European Journal* 12:8434–8442.
3. Elizarov AM (2009) Microreactors for radiopharmaceutical synthesis. *Lab Chip* 9:1326–1333.
4. Sahoo HR, Kralj JG, Jensen KF (2007) Multistep continuous-flow microchemical synthesis involving multiple reactions and separations. *Angew Chem Int Edit* 46:5704–5708.
5. Song H, Chen DL, Ismagilov RF (2006) Reactions in droplets in microfluidic channels. *Angew Chem Int Edit* 45:7336–7356.
6. Lee C-C, et al. (2005) Multistep synthesis of a radiolabeled imaging probe using integrated microfluidics. *Science* 310:1793–1796.
7. Lee JN, Park C, Whitesides GM (2003) Solvent compatibility of Poly(dimethylsiloxane)-based microfluidic devices. *Anal Chem* 75:6544–6554.
8. Fair R (2007) Digital microfluidics: is a true lab-on-a-chip possible? *Microfluid Nanofluid* 3:245–281.
9. Cho SK, Moon H, Kim C-J (2003) Creating, transporting, cutting, and merging liquid droplets by electrowetting-based actuation for digital microfluidic circuits. *Journal of Microelectromechanical systems* 12:70–80.
10. Gong J, Kim C-J (2008) All-electronic droplet generation on-chip with real-time feedback control for EWOD digital microfluidics. *Lab Chip* 8:898–906.
11. Schertzer MJ, Ben-Mrad R, Sullivan PE (2010) Using capacitance measurements in EWOD devices to identify fluid composition and control droplet mixing. *Sensor Actuat B: Chem* 145:340–347.
12. Nelson WC, et al. (2010) Incubated protein reduction and digestion on an electrowetting-on-dielectric digital microfluidic chip for MALDI-MS. *Anal Chem* 82:9932–9937.
13. Chatterjee D, Hetayothin B, Wheeler AR, King DJ, Garrell RL (2006) Droplet-based microfluidics with nonaqueous solvents and solutions. *Lab Chip* 6:199–206.
14. Marchand G, et al. (2008) Organic synthesis in soft wall-free microreactors: real-time monitoring of fluorogenic reactions. *Anal Chem* 80:6051–6055.
15. Phelps ME (2000) Positron emission tomography provides molecular imaging of biological processes. *Proc Natl Acad Sci USA* 97:9226–9233.
16. Kelloff GJ, et al. (2005) Progress and promise of FDG-PET imaging for cancer patient management and oncologic drug development. *Clin Cancer Res* 11:2785–2808.
17. Steel CJ, O'Brien AT, Luthra SK, Brady F (2007) Automated PET radiosyntheses using microfluidic devices. *J Labelled Compd Rad* 50:308–311.
18. Gillies JM, et al. (2006) Microfluidic reactor for the radiosynthesis of PET radiotracers. *Appl Radiat Isotopes* 64:325–332.
19. Miller PW, Long NJ, Vilar R, Gee AD (2008) Synthesis of 11C, 18F, 15O, and 13N radiolabels for positron emission tomography. *Angew Chem Int Edit* 47:8998–9033.
20. Elizarov AM, et al. (2010) Design and optimization of coin-shaped microreactor chips for pet radiopharmaceutical synthesis. *J Nucl Med* 51:282–287.
21. Bejot R, et al. (2011) Batch-mode microfluidic radiosynthesis of N-succinimidyl-4-[^{18}F] fluorobenzoate for protein labelling. *J Labelled Compd Rad* 54:117–122.
22. AGC Chemicals, ASAHI Glass Company, Ltd CYTOP amorphous fluoropolymer., Available at: http://www.bellexinternational.com/products/cytop/pdf/cytop-catalog.pdf [Accessed May 13, 2011].
23. Hamacher K, Coenen HH, Stocklin G (1986) Efficient stereospecific synthesis of No-Carrier-Added 2-[^{18}F]-Fluoro-2-Deoxy-D-Glucose using aminopolyether supported nucleophilic substitution. *J Nucl Med* 27:235–238.
24. Taniguchi T, Torii T, Higuchi T (2002) Chemical reactions in microdroplets by electrostatic manipulation of droplets in liquid media. *Lab Chip* 2:19–23.
25. Nelson WC, Yen M, Keng PY, van Dam MR, Kim C-J (2011) High-pressure EWOD digital microfluidics. (Proceedings of the 16th IEEE International Solid-State Sensors, Actuators and Microsystems, Beijing, China), pp 2932–2935.
26. Dubois P, et al. (2006) Ionic liquid droplet as e-microreactor. *Anal Chem* 78:4909–4917.
27. Kim HW, et al. (2004) Rapid synthesis of [^{18}F]FDG without an evaporation step using an ionic liquid. *Appl Radiat Isotopes* 61:1241–1246.
28. Kim DW, Chi DY (2004) Polymer-supported ionic liquids: imidazolium salts as catalysts for nucleophilic substitution reactions including fluorinations. *Angew Chem Int Edit* 43:483–485.
29. Parker AJ (1969) Protic-dipolar aprotic solvent effects on rates of bimolecular reactions. *Chem Rev* 69:1–32.
30. Cho JS, et al. (2009) Cerenkov radiation imaging as a method for quantitative measurements of beta particles in a microfluidic chip. *Phys Med Biol* 54:6757–6771.
31. Yu S (2006) Review of 18F-FDG synthesis and quality control. *Biomed. Imaging Interv. J*, 2 p:e57.
32. Scott PJH, Kilbourn MR (2007) Determination of residual Kryptofix 2.2.2 levels in [^{18}F]-labeled radiopharmaceuticals for human use. *Appl Radiat Isotopes* 65:1359–1362.
33. Gaylord Chemical Corporation (2005) Dimethyl sulfoxide (DMSO) physical properties. Bulletin #101, 2005.
34. Chen S, Keng PY, van Dam RM, Kim C-J (2011) *Proceedings of the 24th IEEE International Conference on Micro Electro Mechanical Systems* (Institute of Electrical and Electronics Engineers (IEEE)).
35. Loening AM, Gambhir SS (2003) AMIDE: a free software tool for multimodality medical image analysis. *Mol Imaging* 2:131–137.

CHEMISTRY

MEDICAL SCIENCES